



1 **Microbial Membrane Tetraether lipid-inferred paleohydrology and**
2 **paleotemperature of Lake Chenghai during the Pleistocene-Holocene**
3 **transition**

4 Weiwei Sun ^a, Enlou Zhang ^{a,b,*}, Jie Chang ^a, James Shulmeister ^{c,d}, Michael I. Bird ^e,
5 ^f, Cheng Zhao ^{a,b}, Qingfeng Jiang ^g, Ji Shen ^a

6 ^a State Key Laboratory of Lake Science and Environment, Nanjing Institute of
7 Geography and Limnology, Chinese Academy of Sciences, Nanjing 210008, China

8 ^b Center for Excellence in Quaternary Science and Global Change, Chinese Academy
9 of Science, Xian 710061, China

10 ^c School of Earth and Environmental Sciences, The University of Queensland, St
11 Lucia, Brisbane, Qld, 4072, Australia

12 ^d School of Earth and Environment, University of Canterbury, Private Bag 4800,
13 Christchurch, New Zealand

14 ^e ARC Centre of Excellence for Australian Biodiversity and Heritage, James Cook
15 University, PO Box 6811, Cairns, Queensland, 4870, Australia

16 ^f College of Science and Engineering, James Cook University, PO Box 6811, Cairns,
17 Queensland, 4870, Australia

18 ^g School of Geography Sciences, Nantong University, Nantong, 226007, China

19 * Corresponding authors. elzhang@niglas.ac.cn. State Key Laboratory of Lake
20 Science and Environment, Nanjing Institute of Geography and Limnology, Chinese
21 Academy of Sciences, Nanjing 210008, China

22

23

24



25 **ABSTRACT**

26 Over the past few decades, paleoenvironmental studies in the Indian Summer
27 Monsoon (ISM) region have mainly focused on precipitation change, with few
28 published terrestrial temperature records from the region. We analyzed the distribution
29 of isoprenoid glycerol dialkyl glycerol tetraethers (isoGDGTs) in the sediments of
30 Lake Chenghai in southwest China across the Pleistocene–Holocene transition, to
31 extract both regional hydrological and temperature signals for this important transition
32 period. Lake-level was reconstructed from the relative abundance of crenarchaeol in
33 isoGDGTs (%cren) and the crenarchaeol'/crenarchaeol ratio. The %cren-inferred
34 lake-level identified a single lowstand (15.4–14.4 cal ka BP), while the
35 crenarchaeol'/crenarchaeol ratio suggests relatively lower lake-level between
36 15.4–14.4 cal ka BP and 12.5–11.7 cal ka BP, corresponding to periods of weakened
37 ISM during the Heinrich 1 (H1) and Younger Dryas (YD) cold event. A filtered
38 TetraEther indeX consisting of 86 carbon atoms (TEX₈₆ index) revealed that lake
39 surface temperature reached present-day values during the YD cold event, and
40 suggests a substantial warming of ~4 °C from the early Holocene to the mid-Holocene.
41 Our paleotemperature record is generally consistent with other records in southwest
42 China, suggesting that the distribution of isoGDGTs in Lake Chenghai sediments has
43 potential for quantitative paleotemperature reconstruction.

44

45 **Keywords:** Quantitative temperature reconstruction; Lake-level; TEX₈₆; Isoprenoid
46 GDGTs; Lacustrine sediment

47

48

49

50

51



52 **1. Introduction**

53 Precipitation in the Indian summer monsoon (ISM) region has decreased
54 substantially with recent global warming, greatly threatening ecosystem function,
55 water availability and economic security across the region (Sinha et al., 2011; Sinha et
56 al., 2015; Ljungqvist et al., 2016). For example, in 2009-2010 severe droughts
57 occurred in southwest China that reduced food production dramatically (Lü et al.,
58 2012). This has stimulated growing scientific interest in understanding the underlying
59 forcing mechanisms behind climate variability in the ISM region on different
60 time-scale, in order to better predict future monsoonal variations.

61 Over the past two decades, climate evolution in the ISM region since the Last
62 Glacial Maximum has been reconstructed from various paleoclimatic archives,
63 including stalagmites, marine and lacustrine sediments (Dykoski et al., 2005; Rashid
64 et al., 2007; Govil and Divakar Naidu, 2011; Saraswat et al., 2013; Contreras-Rosales
65 et al., 2014; Wang et al., 2014b; Dutt et al., 2015; Wu et al., 2015; Kathayat et al.,
66 2016; Zhang et al., 2017a, 2017b; Li et al., 2018; Zhang et al., 2018; Sun et al., 2019;
67 Zhang et al., 2019). These studies provide evidence that changes in ISM precipitation
68 and temperature were generally synchronous on the orbital- and millennial-scale, with
69 a weakened ISM during cold events, and strengthened ISM during warm intervals.
70 However, there remains a paucity of quantitative reconstructions of both hydrological
71 and thermal parameters from the ISM region (Zhang et al., 2017a; Wu et al., 2018;
72 Ning et al., 2019; Zhang et al., 2019), which hinders our detailed understanding of the
73 dynamics of the ISM and therefore the development of climate models with improved
74 prognostic potential.

75 Pollen, chironomids, alkenone and glycerol dialkyl glycerol tetraethers (GDGTs)
76 have been widely used for the quantitative reconstruction of terrestrial
77 paleotemperature during the Quaternary (Nakagawa et al., 2003, 2006; Blaga et al.,
78 2013; Stebich et al., 2015; Wang et al., 2017b; Zhang et al., 2017a; Sun et al., 2018;
79 Wu et al., 2018; Ning et al., 2019; Tian et al., 2019; Zhang et al., 2019). Isoprenoid
80 GDGTs (isoGDGTs) are a suit of membrane lipids produced by some species of



81 archaea, that are ubiquitous in soils, lacustrine and marine sediments (Schouten et al.,
82 2013). The distribution of isoGDGTs compounds correlates well with surface water
83 temperature, and therefore has great potential for use as a paleotemperature proxy
84 (Schouten et al., 2002; Blaga et al., 2009; Kim et al., 2010; Powers et al., 2010).

85 The TetraEther indeX consisting of 86 carbon atoms (TEX₈₆ index), which
86 represents the relative number of cyclopentane moieties in isoGDGT molecules
87 derived from aquatic Thaumarchaeota, has also been successfully applied as a
88 paleothermometer in large lakes (Tierney et al., 2008; Berke et al., 2012; Blaga et al.,
89 2013; Wang et al., 2015). However, the index may not be a reliable proxy for past
90 temperature in small lakes (Blaga et al., 2009; Powers et al., 2010; Sinninghe Damsté
91 et al., 2012a). In addition, the proportion of crenarchaeol in isoGDGTs has been
92 suggested to be a lake-level proxy due to a preference of the producer of this
93 compound for a niche above the oxycline in the upper part of the water column in
94 lacustrine systems (Wang et al., 2014a; Wang et al., 2017a; Wang et al., 2019). In this
95 study, we present an isoGDGT record from Lake Chenghai in the southwest China.
96 We use the results to test the reliability of isoGDGT-based proxies as lake-level and
97 temperature indicators, by comparing our results with other paleoenvironmental
98 records from adjacent areas.

99

100 **2. Materials and methods**

101 *2.1. Regional setting*

102 Lake Chenghai (26°27'-26°38'N, 100°38'-100°41'E, Fig. 1A) is a tectonic lake
103 located in Yongsheng County in Yunnan Province (Wang and Dou, 1998). The present
104 elevation of the lake-level is ~1500 m above sea level (a.s.l.), and the maximum depth
105 is ~35 m with a mean depth of ~20 m. The lake has a surface area of ~77 km² with a
106 catchment of ~318 km² (Wu et al., 2004). The annual mean lake surface temperature
107 (LST) is ~16 °C (Wan et al., 2005). The lake water is slightly brackish (average=
108 ~1‰) and alkaline (average pH= ~8). There are no perennial inlets or outflow streams



109 at present, and the lake is mainly maintained by direct precipitation and groundwater
110 (Wan et al., 2005). Lake Chenghai was linked to the Jinsha River via the Haikou
111 River during the Ming Dynasty (1368-1644 CE), but became a closed lake in the
112 1690s CE when a dam (~1540 m a.s.l.) was constructed on its southern side (Wang
113 and Dou, 1998).

114 The lake basin is surrounded by mountains ranging from 2300-4000 m a.s.l.
115 Topsoil types include lateritic red earths and mountain red brown soils (Wang and
116 Dou, 1998). The region is mainly affected by a warm-humid monsoonal airflow from
117 the tropical Indian Ocean from June to September, and by the southern branch of the
118 Northern Hemisphere westerly jet between October and May (Wang and Dou, 1998).
119 Observed climatic data spanning the past 30 years from the Yongsheng meteorological
120 station (26.68 °N, 100.75 °E; elevation of 2130 m a.s.l.) indicate a mean annual
121 temperature of 14 °C, an annual precipitation of 660 mm, ~80% of which falls from
122 June to September.

123 2.2. *Sampling and dating*

124 An 874-cm-long sediment core was retrieved at 26°33'29.4"N, 100°39'6.7"E
125 using a UWITEC coring platform system with a percussion corer in July 2016 CE.
126 The water depth was 30 m. The sediment cores were split longitudinally,
127 photographed and then sectioned at a 1-cm interval in the laboratory, and the samples
128 stored at 4 °C until analysis.

129 The chronology was established using accelerator mass spectrometry (AMS) ¹⁴C
130 dating of terrestrial plant macrofossils and charcoal (Sun et al., 2019). Macrofossils of
131 leaves, woody stems and charcoal were hand-picked under the microscope. Eight
132 dates covering the period from the last deglaciation to early Holocene were obtained.
133 The analyses were performed at the Beta Analytic Radiocarbon Dating Laboratory in
134 Miami, USA. The age model was developed utilizing Bacon, implemented in R 3.1.0
135 at 5-cm intervals (Blaauw and Andres Christen, 2011; R Development Core Team,
136 2013). All AMS ¹⁴C dates were calibrated to calendar years before present (0 BP



137 =1950 CE) using the program Calib 7.1 and the IntCal13 calibration data set (Reimer
138 et al., 2013). The basal mean weighted age is ~15.6 cal ka BP (Fig. 2, Sun et al.,
139 2019).

140 2.3. Lipid extraction and analysis

141 After freeze-drying, a total of 102 samples at 4-cm interval over the
142 Pleistocene-Holocene transition were collected for GDGT analysis, and this was
143 increased to 1-cm resolution across 792-806 cm span due to the low sedimentation
144 rate over this interval. A ~4 g aliquot of each sample was extracted ultrasonically (4
145 times) with a mixture of dichloromethane and methanol (9:1, v/v). The supernatants
146 were condensed and base hydrolyzed in a 1 M KOH/methanol solution. The neutral
147 fractions were then separated into apolar and polar fractions on a silica gel column,
148 using *n*-hexane and methanol, respectively. The polar fraction containing the GDGTs
149 was concentrated and filtered through 0.45 µm polytetrafluoroethylene syringe filters
150 using *n*-hexane/ isopropanol (99:1 v/v). These fractions were then dried in N₂ and
151 stored at -20 °C until further analysis.

152 GDGTs were analyzed using an Agilent 1200 series high performance liquid
153 chromatography-atmospheric pressure chemical ionization-mass spectrometer
154 (HPLC- APCI- MS), following the procedure of Yang et al. (2015) at the Institute of
155 Tibetan Plateau Research, Chinese Academy of Sciences. Briefly, the GDGTs were
156 separated using three silica columns in tandem (150 mm× 2.1 mm, 1.9 µm; Thermo
157 Finnigan, U.S.A.), maintained at 40 °C. The elution gradients were 84% *n*-hexane (A):
158 16% ethyl acetate for 5 min, 84/16 to 82/18 A/B for another 60 min, then to 100% B
159 for 21 min and kept for 4 min, followed by a return to 84/16 A/B for 30 min. The total
160 flow rate of pump A and pump B was maintained at 0.1 ml/min. The APCI-MS
161 conditions were: vaporizer pressure 60 psi, vaporizer temperature 400 °C, drying gas
162 flow 6 L/min and temperature 200 °C, capillary voltage 3500 V and corona current 5
163 µA (~3200 V). Selected ion monitoring (SIM) mode was performed to target specific
164 *m/z* values for each GDGT compound, including 1302 (GDGT-0), 1300 (GDGT-1),
165 1298 (GDGT-2), 1296 (GDGT-3), 1294 (crenarchaeol), 1292 (crenarchaeol'), 1050



166 (IIIa, IIIa'), 1048 (IIIb, IIIb'), 1046 (IIIc, IIIc'), 1036 (IIa, IIa'), 1034 (IIb, IIb'), 1032
167 (IIc, IIc'), 1022 (Ia), 1020 (Ib) and 1018 (Ic). The chemical structures of these
168 compounds are presented in Supplementary Fig. S1. The results are presented as the
169 fractional of the sum of the isoGDGTs or the sum of the branched GDGTs (brGDGTs),
170 based on the integration of the peak areas of the [M+H]⁺ ions.

171 2.4. Index calculation and temperature reconstruction

172 The percentage of each isoGDGT (X) was calculated according to the following
173 equation:

$$174 \quad \%X = \frac{X}{(\text{GDGT-0} + \text{GDGT-1} + \text{GDGT-2} + \text{GDGT-3} + \text{crenarchaeol} + \text{crenarchaeol}')} \quad (1)$$

176 The TEX₈₆ index was defined by Schouten et al. (2002) as follows:

$$177 \quad \text{TEX}_{86} = \frac{(\text{GDGT-2} + \text{GDGT-3} + \text{crenarchaeol}')}{(\text{GDGT-1} + \text{GDGT-2} + \text{GDGT-3} + \text{crenarchaeol}')} \quad (2)$$

179 TEX₈₆-inferred LST was calculated using the global lake calibration of
180 Castañeda and Schouten (2015):

$$181 \quad \text{LST} = 49.03 \times \text{TEX}_{86} - 10.99 \quad (r^2 = 0.88, n=16, \text{RMSE} = 3.1 \text{ } ^\circ\text{C}) \quad (3)$$

182 The ratio of branched to isoprenoid tetraethers (BIT index), used as an indicator
183 of soil organic matter input and as a test of the utility of the TEX₈₆ paleotemperature
184 proxy, was calculated following Hopmans et al. (2004):

$$185 \quad \text{BIT} = \frac{(\text{Ia} + \text{IIa} + \text{IIa}' + \text{IIIa} + \text{IIIa}')}{(\text{Ia} + \text{IIa} + \text{IIa}' + \text{IIIa} + \text{IIIa}' + \text{crenarchaeol})} \quad (4)$$

187

188 3. Results

189 A wide variety of isoGDGT compositions is present in the sediments of Lake
190 Chenghai. As illustrated in Fig. 3, the relative abundances of crenarchaeol (%cren)
191 ranged from 2.4-61.3% with a mean of 52.4%. The %cren values were relatively low



192 and highly variable during 15.4-14.4 cal ka BP, ranging from 1.8-32.0%, with a mean
193 of 11.6%. By contrast, the values were relatively stable during 14.4-7.0 cal ka BP,
194 ranging from 41.8-61.3% with a mean of 58.3%. The relative abundances of its
195 regioisomer, crenarchaeol', had a mean of 1.7%. The ratios of
196 crenarchaeol'/crenarchaeol were highly variable during 15.4-14.4 cal ka BP with a
197 mean of 0.07. After this time, the values gradually decrease during 14.4-11.7 cal ka
198 BP with a minor reversal during 12.5-11.7 cal ka BP, where the ratio averaged 0.05.
199 The crenarchaeol'/crenarchaeol ratios were generally stable and fluctuated around
200 0.03 during the period 11.8-7.0 cal ka BP.

201 The relative abundances of GDGT-0 (%GDGT-0) showed a significant negative
202 correlation with the reciprocal of %cren ($r^2 = 0.98$, $p < 0.001$). The %GDGT-0 values
203 had a mean of 74.0% during 15.4-14.4 cal ka BP and a mean of 19.6% during the
204 14.4-7.0 cal ka BP interval. The ratios of GDGT-0/crenarchaeol were generally >2
205 during the period 15.4-14.4 cal ka BP, ranging from 1.4-49.9 with a mean of 16.7, and
206 all <2 from 14.4-7.0 cal ka BP. The relative abundance of GDGT-1, GDGD-2 and
207 GDGT-3 were generally low in the sediments, with a mean of 8.9, 9.2, and 1.3,
208 respectively.

209 The TEX_{86} values were also highly variable during 15.4-14.4 cal ka BP period,
210 ranging from 0.36-0.68 with a mean of 0.54. Thereafter the values generally followed
211 an increasing trend, ranging from 0.49-0.63 with a mean of 0.58. The BIT values
212 exhibited a significant negative correlation with cren% values ($r^2 = 0.94$, $p < 0.001$),
213 ranging from 0.39-0.99 with a mean of 0.54. An abrupt decrease from 0.96 to 0.52
214 occurred at 14.4 cal ka BP. After this time, the BIT values gradually decreased to a
215 minimum value at 9.3 cal ka BP, and fluctuated thereafter around 0.48 during 9.3-7.0
216 cal ka BP.

217

218 **4. Discussion**

219 *4.1. Environmental significances of the isoGDGT-based proxies*



220 Crenarchaeol and its regioisomer are considered to be produced specifically by
221 mesophilic Thaumarchaeota in aquatic environments (Schouten et al., 2002; Schouten
222 et al., 2013). In marine conditions, Thaumarchaeota have a physiological mechanism
223 to increase the weighted average number of cyclopentane rings in their membrane
224 lipids with growth temperature, thus a significant linear correlation is found between
225 TEX₈₆ values and mean annual sea surface temperature (Schouten et al., 2002). In the
226 studies of lacustrine systems, the temperature calibration of TEX₈₆ has been found to
227 be nearly identical to the marine calibration, suggesting that the paleothermometer can
228 also be applied in lacustrine sediments (Powers et al., 2004; Blaga et al., 2009;
229 Powers et al., 2010; Castañeda and Schouten, 2011). In addition, aquatic
230 Thaumarchaeota are nitrifiers, that prefer to live above the oxycline of relatively deep
231 lakes, as has been observed by a range of lipid biomarker and DNA based
232 investigations of vertical changes in archaea communities in lake water columns
233 (Sinninghe Damsté et al., 2009; Blaga et al., 2011; Schouten et al., 2012; Buckles et
234 al., 2013; Meegan Kumar et al., 2019).

235 Some Thaumarchaeota are considered to be suppressed by a high light level,
236 which consequently might also prohibit them from thriving right near the surface
237 layer of lake water (Schouten et al., 2013). In addition, Thaumarchaeota are
238 chemoautotrophic and thrive predominantly near the oxycline in stratified lakes,
239 mainly due to the release of ammonia derived from descending particulate organic
240 matter that is recycled primarily by photoautotrophs or heterotrophs in the photic zone
241 (Tierney et al., 2010). Furthermore, mixing of the water column will be much more
242 frequent at lowstand conditions (Filippi and Talbot, 2005), and therefore periodically
243 or permanently oxic, high nutrient availability water and enhanced nitrogen cycling
244 would be likely result in a relatively lower production of crenarchaeol. Therefore, the
245 cren% value measure in lacustrine sediments has been proposed to be a potential
246 proxy for lake level change, with high values indicating highstand and deep lake
247 status, while low values reflecting lowstand and shallow lake status (Wang et al.,
248 2014a; Wang et al., 2017a; Wang et al., 2019).



249 Although TEX_{86} and $\text{cren}\%$ show great potential as paleotemperature and
250 paleo-lake-level proxies, they may be significantly biased when a substantial amount
251 of soil and/or methanogenic archaea isoGDGTs are identified in the same lacustrine
252 sediment (Weijers et al., 2006; Blaga et al., 2009; Powers et al., 2010; Wang et al.,
253 2019). BIT index values are generally >0.90 in soils, whereas values are close to zero
254 for large lake sediments (Hopmans et al., 2004; Weijers et al., 2006). In this study,
255 Lake Chenghai sediment the BIT index values range from 0.39-0.99, indicating that a
256 considerable proportion of isoGDGTs could derive from soils. However, recent
257 studies of modern processes in a wide variety of lakes have suggested that at least
258 partly branched GDGTs are generated by *in-situ* production (Blaga et al., 2010;
259 Tierney et al., 2010; Pearson et al., 2011; Hu et al., 2016; Dang et al., 2018; Russell et
260 al., 2018). Therefore, *in-situ* production of branched GDGTs in Lake Chenghai cannot
261 be fully excluded.

262 It has also been shown that crenarchaeol' is only present in low abundance in
263 most Thaumarchaeota except for the group I.1b Thaumarchaeota, where it is one of
264 the major GDGTs (Kim et al., 2012; Sinninghe Damsté et al., 2012b). The
265 crenarchaeol'/crenarchaeol ratios for enrichment cultures of group I.1a aquatic
266 Thaumarchaeota are typically 0.01-0.04, however, for group I.1b Thaumarchaeota
267 enriched from soils the crenarchaeol'/crenarchaeol ratios are around 0.21 and
268 substantially higher (Pitcher et al., 2011; Sinninghe Damsté et al., 2012a). This
269 suggests that the observed down-core changes in crenarchaeol'/crenarchaeol ratios
270 may be due to relatively high contributions of group I.1b Thaumarchaeota from soils
271 during 15.4-11.8 cal ka BP, and that these dominate the contributions of isoGDGTs
272 derived from aquatic group I.1a Thaumarchaeota during the period from 11.8-7.0 cal
273 ka BP.

274 The TEX_{86} and $\text{cren}\%$ measures might also be affected by methanogenic and
275 methanotrophic archaea because methanogenesis is the dominant anaerobic metabolic
276 pathway in freshwater ecosystems (Blaga et al., 2009; Dang et al., 2016; Yao et al.,
277 2019). Crenarchaeol and GDGT-0 can be derived from Group I Thaumarchaeota,



278 whereas methanogens synthesize GDGT-0, but no crenarchaeol. On this basis, the
279 ratio of GDGT-0/crenarchaeol has been proposed to evaluate the influence of
280 methanogenesis on the distribution of isoGDGTs in lacustrine sediments (Blaga et al.,
281 2009). The ratio typically varies between 0.2 and 2 in group I Thaumarchaeota, thus a
282 value >2 is generally thought to reflect a substantial contribution from methanogens
283 to the total isoGDGT (Schouten et al., 2002; Blaga et al., 2009). Therefore, higher
284 GDGT-0/crenarchaeol values suggest that methanogenic and methanotrophic archaeal
285 were also likely to be an important source of GDGTs in some of Lake Chenghai
286 sediments during 15.4-14.4 cal ka BP.

287 4.2. Assessment of isoGDGT-based lake-level proxy

288 Environmental changes at Lake Chenghai as inferred from %cren,
289 crenarchaeol'/crenarchaeol ratio, the BIT index and GDGT-0/crenarchaeol ratio
290 during the period from the last deglaciation to the early Holocene are illustrated in Fig.
291 4. The relatively low %cren and high GDGT-0/crenarchaeol values during 15.4-14.4
292 cal ka BP suggest that the Thaumarchaeota were mainly suppressed by methanogenic
293 and methanotrophic archaeal. Deep lake conditions and thermal stratification have
294 also been suggested as important in influencing the Thaumarchaeota's growth, while
295 any increase in water column turbulence would have negatively affected them
296 (Tierney et al., 2010). Thus the abrupt increase in %cren values at 14.4 cal ka BP
297 suggest a lowland of Lake Chenghai during 15.4-14.4 cal ka BP, and a highstand
298 period thereafter.

299 The lowstand period is consistent in timing with the stable oxygen isotope ($\delta^{18}\text{O}$)
300 record of authigenic carbonates derived from the same core (Fig. 4e, Sun et al., 2019),
301 speleothem $\delta^{18}\text{O}$ records from Mawmluh Cave and Bittoo Cave in north India (Fig. 4f,
302 Dutt et al., 2015; Kathayat et al., 2016), and Donnge Cave in southwest China
303 (Dykoski et al., 2005), which all record a substantial positive shift in $\delta^{18}\text{O}$ values at
304 that time. Speleothem $\delta^{18}\text{O}$ records in the ISM region are used as a rainfall amount
305 proxy, tracking changes in monsoon intensity (Dykoski et al., 2005; Cheng et al.,
306 2012; Dutt et al., 2015). Therefore, the lowstand of Lake Chenghai during 15.4-14.4



307 cal ka BP implies a weakened ISM during the Heinrich 1 (H1) cold event, consistent
308 with other evidence.

309 Low lake-levels during the H1 cold event are also indicated by several previous
310 paleolimnological studies from the Yunnan Plateau, within the uncertainties of the age
311 model. Diatom and grain-size records from Lake Tengchongqinghai show a
312 significant decrease in acidophilous diatom species and an increase in the grain-size
313 of mineral particles from 18.5 to 15.0 cal ka BP, suggesting that the climate was driest
314 and the ISM was at its weakest since the last deglaciation (Fig. 4g, Zhang et al., 2017b;
315 Li et al., 2018). Similarly, an increase in $>30\ \mu\text{m}$ grain-size particles in the late glacial
316 sediments from Lake Xingyun reflects a period of abrupt weak ISM during the H1
317 cold event (Wu et al., 2015). In Lake Lugu, the loss of the planktonic diatoms and a
318 switch to small *Fragilaria* spp. suggest a weaker stratification during 24.5-14.5 cal ka
319 BP, which might also correspond to low lake-level at that time (Wang et al., 2014b).

320 Lake Chenghai lake-level does not seem to reduce during the Younger Dryas
321 (YD) cold event, which is also recognized as a millennial-scale period of weak ISM
322 (Dutt et al., 2015; Dykoski et al., 2005; Kathayat et al., 2016; Sun et al., 2019). In
323 contrast, a low lake-level signal is observed in the $\delta^{18}\text{O}$ record of authigenic
324 carbonates from Lake Chenghai (Sun et al., 2019). In addition, increased lake water
325 alkalinity and decreased lake-level are also recorded in the diatom and grain-size
326 proxy records during 12.8-11.1 cal ka BP of Lake Tengchongqinghai (Fig. 4g, Zhang
327 et al., 2017b; Li et al., 2018). The differences in lake hydrological conditions to the
328 YD weak ISM inferred from different lake sediment records is possibly due to
329 differences in the sensitivity of the proxy to lake-level variation in the case of Lake
330 Chenghai.

331 The $\delta^{18}\text{O}$ record of authigenic carbonates from Lake Chenghai and speleothem
332 $\delta^{18}\text{O}$ records in the ISM region suggest that the weakening of the ISM during the YD
333 was less marked than that occurring during the H1 event, in turn suggesting that
334 lake-levels in southwest China may have been higher during the YD than the H1
335 event (Dykoski et al., 2005; Dutt et al., 2015; Kathayat et al., 2016; Sun et al., 2019;



336 Zhang et al., 2019). For the %cren proxy, we note that the values are significantly
337 correlated to the logarithm of depth in Asian lakes ($\%cren = 19.59 \times \log(\text{depth}) + 9.23$),
338 suggesting that %cren may be less sensitive to water depth variation when the
339 lake-level is relatively high (Wang et al., 2019). It is also worth noting that the
340 crenarchaeol'/crenarchaeol ratios were not only relatively higher during the H1 cold
341 event, but also showed a minor reversal during the YD cold event. These results are
342 consistent with group I.1b Thaumarchaeota being an important source of isoGDGTs
343 in some small lakes and to the nearshore area of large lakes (Wang et al., 2019).

344 4.3. Warming in the early Holocene

345 Robust application of the TEX₈₆-based paleotemperature calibration critically
346 depends on the assumption that the isoGDGTs used for calculation of TEX₈₆ values
347 are mainly been derived from group I.1a in the water column (Blaga et al., 2009;
348 Castañeda and Schouten, 2011; Powers et al., 2010; Sinninghe Damsté et al., 2012a).
349 Since the influence of methanogenic archaea in the water column or archaea in the
350 catchment soils have been recognized, Lake Chenghai sediments with BIT
351 values >0.5 and/or GDGT-0/crenarchaeol ratio >2 are excluded from the discussion
352 below (Powers et al., 2010; Castañeda and Schouten, 2015). 57 samples remain that
353 have isoGDGT distributions consistent with their dominant source being the aquatic
354 Thaumarchaeota, most of these being from the time interval between 11.7-8.2 cal ka
355 BP, and only a few from the early YD period (n=2) and 8.2-7.0 cal ka BP (n= 6).
356 Using Equation 4 developed by Castañeda and Schouten (2015) to calculate mean
357 LST, yielded LST values from 15.7-20.1 °C, with a mean of 17.9 °C (Fig. 5a).

358 LST was ~15.8 °C during the early YD period, a temperature approaching the
359 16 °C observed in the present Lake Chenghai. Following the YD cold event, LST
360 rapidly increased from 16.2 °C at 11.2 cal ka BP to 18.2 °C at 11.0 cal ka BP, and LST
361 ranged from 16.8 °C to 20.1 °C with a an increasing trend observed during the
362 11.0-7.0 cal ka BP interval. This result is consistent with other recent reconstructed
363 mean annual temperatures in southwest China, which show the temperatures during
364 the YD cold event were generally similar to the present-day value, and the middle



365 Holocene was generally warmer than the early Holocene (Ning et al., 2019; Tian et al.,
366 2019). For example, mean annual temperatures were 1.3 °C higher between 7.6 and
367 5.5 cal ka BP than during 9.4-7.6 cal ka BP as inferred from the branched GDGT
368 record from Lake Ximenglongtan in southwest China (Fig. 5d, Ning et al., 2019).
369 Furthermore, the July temperature derived from the chironomid record from Lake
370 Tiancai and the pollen record from Lake Xingyun also show similar values during the
371 YD cold event with that of the present-day (Fig. 5b and c, Wu et al., 2018; Zhang et
372 al., 2019). The pollen record from Lake Xingyun in southwest China suggested that
373 the July temperatures remained high values at ~25.5 °C during 8.0-5.5 cal ka BP, and
374 ~1.6 °C higher than those during the early Holocene (Wu et al., 2018). However, July
375 temperatures reconstructed from Lake Tiancai in southwest China display much lower
376 amplitude of change, being only 0.3 °C higher during the mid-Holocene than the early
377 Holocene (Zhang et al., 2017a).

378 Temperature in areas affected by the East Asian summer monsoon was more
379 sensitive to high latitude climate change than in the ISM region. The mean annual
380 temperature was ~8.5 °C cooler than present day during 12.3-11.3 cal ka BP in
381 southwest Japan as inferred from the pollen record from Lake Suigetsu, with the
382 variation larger in winter than summer (Fig. 5f, Nakagawa et al., 2003, 2006). The
383 mean annual temperature estimated from the branched GDGTs record from the
384 Shuizhuyang peat bog in southeast China dropped to 10.3 °C during the YD cold
385 period, ~5.5 °C cooler than present-day (Wang et al., 2017b). In addition, a pollen
386 record from Lake Sihailongwan in northeast China suggests a cool mixed forest
387 biome was the dominant vegetation type during the late YD period, leading to the
388 calculation of a mean July temperature of ~15-16 °C, 5-6 °C cooler than modern July
389 temperature (Fig. 5e, Stebich et al., 2015). The summer LST of Lake Sihailongwan
390 reconstructed from long-chain alkenones shows the average temperature was
391 ~14.2 °C during the YD event, ~4.3 °C cooler than the modern instrumental water
392 temperature (Sun et al., 2018). Following the YD cold event, the pollen record from
393 Lake Sihailongwan in northeast China suggests that the July temperatures gradually



394 increased from 18.0 °C at 11.4 cal ka BP to 26.5 °C at 8.1 cal ka BP, and remained at
395 generally high values (>25.0 °C) during the mid-Holocene (Stebich et al., 2015). The
396 branched GDGTs record from Gushantu peat bog in northeast China also shows the
397 highest mean annual temperatures occurred between 8.0 and 6.8 cal ka BP (Zheng et
398 al., 2018). The regionally warmer mid-Holocene is considered to be related to the
399 persistence of remnants of the Northern Hemisphere ice-sheets during the early
400 Holocene, which slowed down the Atlantic Meridional overturning circulation and
401 enhanced the westerlies, resulting in lower temperatures across the downstream
402 Eurasian continent (Zhang et al., 2017a; Wu et al., 2018; Ning et al., 2019).

403

404 **5. Conclusions**

405 The record of isoGDGTs in the sediments of Lake Chenghai in southwest China
406 presented in this study allows us to test the ability of isoGDGT-based proxies in the
407 ISM region to reconstruct lake-level and temperature during the Pleistocene-Holocene
408 transition. The lake-level history inferred from %cren shows a relative lowstand of
409 Lake Chenghai during 15.4-14.4 cal ka BP, corresponding to a period of weakened
410 ISM during the H1 cold event. The indistinct signal of lake-level variation during the
411 YD cold event may be due to the %cren proxy not being sensitive to lake-level
412 change when the lake was relatively full. By contrast, the crenarchaeol'/crenarchaeol
413 ratios suggest group I.1b Thaumarchaeota being an important source of isoGDGTs
414 and the lake level was low during the YD cold event. After filtering for the influence
415 of isoGDGTs derived from soils in the surrounding catchment and methanogens, the
416 TEX₈₆ paleothermometry revealed that the LST of Lake Chenghai was similar to the
417 present-day value during the YD cold event and experienced a substantial warming of
418 ~4 °C from the early-Holocene to the mid-Holocene. Overall, our results show that
419 the distribution of isoGDGTs in Lake Chenghai sediments do have potential for
420 quantitative paleotemperature reconstruction once potential underlying biases are
421 properly constrained.



422

423 **Data availability.**

424 All data in this study will be made available on request.

425 **Author contributions.**

426 W.S and E.Z designed the study, W.S performed the fieldwork and lab analysis. W.S
427 and E.Z led the writing of the paper, J.C, J. S, M.I.B, C.Z, Q.J and J.S contributed to
428 data interpretation and paper writing. All authors contributed to discussions and
429 writing of the manuscript. The authors declare that they have no competing financial
430 interests.

431 **Competing interests.**

432 The authors declare that they have no conflict of interest.

433 **Acknowledgments**

434 We thank Dr. R. Chen and D. Ning for field assistance and laboratory analysis. The
435 research was supported by the found from the program of Global Change and
436 Mitigation (2016YFA0600502), the National Natural Science Foundation of China
437 (41702183 and 41572337), and the fund from State Key Laboratory of Lake Science
438 and Environment (2016SKL003).

439

440 **References**

- 441 Berke, M.A., Johnson, T.C., Werne, J.P., Schouten, S., Sinninghe Damsté J.S.: A
442 mid-Holocene thermal maximum at the end of the African Humid Period. *Earth*
443 *Planet. Sc. Lett.* 351-352, 95-104, DOI: 10.1016/j.epsl.2012.07.008, 2012.
- 444 Blaauw, M., Andres Christen, J.: Flexible paleoclimate age-depth models using an
445 autoregressive gamma process. *Bayesian. Anal.* 6, 457-474,
446 DOI: 10.1214/11-BA618, 2011.
- 447 Blaga, C.I., Reichart, G.-J., Heiri, O., Sinninghe Damsté J.S.: Tetraether membrane



- 448 lipid distributions in water-column particulate matter and sediments: a study of
449 47 European lakes along a north–south transect. *J. Paleolimnol.* 41, 523-540,
450 DOI: 10.1007/s10933-008-9242-2, 2009.
- 451 Blaga, C.I., Reichart, G.-J., Lotter, A.F., Anselmetti, F.S., Sinninghe Damsté J.S.: A
452 TEX₈₆ lake record suggests simultaneous shifts in temperature in Central Europe
453 and Greenland during the last deglaciation. *Geophys. Res. Lett.* 40, 948-953,
454 DOI: 10.1002/grl.50181, 2013.
- 455 Blaga, C.I., Reichart, G.-J., Vissers, E.W., Lotter, A.F., Anselmetti, F.S., Sinninghe
456 Damsté J.S.: Seasonal changes in glycerol dialkyl glycerol tetraether
457 concentrations and fluxes in a perialpine lake: Implications for the use of the
458 TEX₈₆ and BIT proxies. *Geochim. Cosmochim. Ac.* 75, 6416-6428, DOI:
459 10.1016/j.gca.2011.08.016, 2011.
- 460 Blaga, C.I., Reichart, G.J., Schouten, S., Lotter, A.F., Werne, J.P., Kosten, S., Mazzeo,
461 N., Lacerot, G., Damste, J.S.S.: Branched glycerol dialkyl glycerol tetraethers in
462 lake sediments: Can they be used as temperature and pH proxies? *Org. Geochem.*
463 41, 1225-1234, DOI: 10.1016/j.orggeochem.2010.07.002, 2010.
- 464 Buckles, L.K., Villanueva, L., Weijers, J.W.H., Verschuren, D., Damsté J.S.S.:
465 Linking isoprenoidal GDGT membrane lipid distributions with gene abundances
466 of ammonia-oxidizing Thaumarchaeota and uncultured crenarchaeotal groups in
467 the water column of a tropical lake (Lake Challa, East Africa). *Environ.l*
468 *Microbiol.* 15, 2445-2462, DOI: 10.1111/1462-2920.12118, 2013.
- 469 Castañeda, I.S., Schouten, S.: A review of molecular organic proxies for examining
470 modern and ancient lacustrine environments. *Quaternary. Sci. Rev.* 30,
471 2851-2891, DOI: 10.1016/j.quascirev.2011.07.009, 2011.
- 472 Castañeda, I.S., Schouten, S.: Corrigendum to “A review of molecular organic proxies
473 for examining modern and ancient lacustrine environments” [*Quat. Sci. Rev.* 30
474 (2011) 2851–2891]. *Quaternary. Sci. Rev.* 125, 174-176, DOI:
475 10.1016/j.quascirev.2015.07.020, 2015.
- 476 Cheng, H., Sinha, A., Wang, X., Cruz, F.W., Edwards, R.L.: The Global
477 Paleomonsoon as seen through speleothem records from Asia and the Americas.



- 478 Clim. Dynam. 39, 1045-1062, DOI: 10.1007/s00382-012-1363-7, 2012.
- 479 Contreras-Rosales, L.A., Jennerjahn, T., Tharammal, T., Meyer, V., Lückge, A., Paul,
480 A., Schefuß E.: Evolution of the Indian Summer Monsoon and terrestrial
481 vegetation in the Bengal region during the past 18 ka. Quaternary. Sci. Rev. 102,
482 133-148, DOI: 10.1016/j.quascirev.2014.08.010, 2014.
- 483 Dang, X., Ding, W., Yang, H., Pancost, R.D., Naafs, B.D.A., Xue, J., Lin, X., Lu, J.,
484 Xie, S.: Different temperature dependence of the bacterial brGDGT isomers in
485 35 Chinese lake sediments compared to that in soils. Org. Geochem., DOI:
486 10.1016/j.orggeochem.2018.02.008, 2018.
- 487 Dang, X.Y., Xue, J.T., Yang, H., Xie, S.C.: Environmental impacts on the distribution
488 of microbial tetraether lipids in Chinese lakes with contrasting pH: Implications
489 for lacustrine paleoenvironmental reconstructions. Sci. China. Earth. Sci. 59,
490 939-950, DOI: 10.1007/s11430-015-5234-z, 2016.
- 491 Dutt, S., Gupta, A.K., Clemens, S.C., Cheng, H., Singh, R.K., Kathayat, G., Edwards,
492 R.L.: Abrupt changes in Indian summer monsoon strength during 33,800 to
493 5500 years B.P. Geophys. Res. Lett. 42, 5526-5532, DOI:
494 10.1002/2015GL064015, 2015.
- 495 Dykoski, C.A., Edwards, R.L., Cheng, H., Yuan, D., Cai, Y., Zhang, M., Lin, Y., Qing,
496 J., An, Z., Revenaugh, J.: A high-resolution, absolute-dated Holocene and
497 deglacial Asian monsoon record from Dongge Cave, China. Earth. Planet. Sc.
498 Lett. 233, 71-86, DOI: 10.1016/j.epsl.2005.01.036, 2005.
- 499 Filippi, M.L., Talbot, M.R.: The palaeolimnology of northern Lake Malawi over the
500 last 25 ka based upon the elemental and stable isotopic composition of
501 sedimentary organic matter. Quaternary. Sci. Rev. 24, 1303-1328, DOI:
502 10.1016/j.quascirev.2004.10.009, 2005.
- 503 Govil, P., Divakar Naidu, P.: Variations of Indian monsoon precipitation during the
504 last 32 kyr reflected in the surface hydrography of the Western Bay of Bengal.
505 Quaternary. Sci. Rev. 30, 3871-3879, DOI: 10.1016/j.quascirev.2011.10.004,
506 2011.
- 507 Hopmans, E.C., Weijers, J.W.H., Schefuss, E., Herfort, L., Damste, J.S.S., Schouten,



- 508 S.: A novel proxy for terrestrial organic matter in sediments based on branched
509 and isoprenoid tetraether lipids. *Earth. Planet. Sc. Lett.* 224, 107-116, DOI:
510 10.1016/j.epsl.2004.05.012, 2004
- 511 Hu, J., Zhou, H., Peng, P.a., Spiro, B.: Seasonal variability in concentrations and
512 fluxes of glycerol dialkyl glycerol tetraethers in Huguangyan Maar Lake, SE
513 China: Implications for the applicability of the MBT-CBT paleotemperature
514 proxy in lacustrine settings. *Chem. Geol.* 420, 200-212, DOI:
515 10.1016/j.chemgeo.2015.11.008, 2016.
- 516 Kathayat, G., Cheng, H., Sinha, A., Spätl, C., Edwards, R.L., Zhang, H., Li, X., Yi, L.,
517 Ning, Y., Cai, Y., Lui, W.L., Breitenbach, S.F.M.: Indian monsoon variability on
518 millennial-orbital timescales. *Sci. Rep-UK.* 6, DOI: 10.1038/srep24374, 2016.
- 519 Kim, J.-G., Jung, M.-Y., Park, S.-J., Rijpstra, W.I.C., Sinninghe Damst é J.S., Madsen,
520 E.L., Min, D., Kim, J.-S., Kim, G.-J., Rhee, S.-K.: Cultivation of a highly
521 enriched ammonia-oxidizing archaeon of thaumarchaeotal group I.1b from an
522 agricultural soil. *Environ. Microbiol.* 14, 1528-1543, DOI:
523 10.1111/j.1462-2920.2012.02740.x, 2012.
- 524 Kim, J.-H., van der Meer, J., Schouten, S., Helmke, P., Willmott, V., Sangiorgi, F.,
525 Ko ç N., Hopmans, E.C., Damst é J.S.S.: New indices and calibrations derived
526 from the distribution of crenarchaeal isoprenoid tetraether lipids: Implications for
527 past sea surface temperature reconstructions. *Geochim. Cosmochim. Ac.* 74,
528 4639-4654, DOI: 10.1016/j.gca.2010.05.027, 2010.
- 529 Li, Y., Chen, X., Xiao, X., Zhang, H., Xue, B., Shen, J., Zhang, E.: Diatom-based
530 inference of Asian monsoon precipitation from a volcanic lake in southwest
531 China for the last 18.5 ka. *Quaternary. Sci. Rev.* 182, 109-120, DOI:
532 10.1016/j.quascirev.2017.11.021, 2018.
- 533 Ljungqvist, F.C., Krusic, P.J., Sundqvist, H.S., Zorita, E., Brattström, G., Frank, D.:
534 Northern Hemisphere hydroclimate variability over the past twelve centuries.
535 *Nature* 532, 94-98, DOI: 10.1038/nature17418, 2016.
- 536 Lü J., Ju, J., Ren, J., Gan, W.: The influence of the Madden-Julian Oscillation activity
537 anomalies on Yunnan's extreme drought of 2009–2010. *Sci. China. Earth. Sci.* 55,



- 538 98-112, DOI: 10.1007/s11430-011-4348-1, 2012.
- 539 Meegan Kumar, D., Woltering, M., Hopmans, E.C., Sinninghe Damsté J.S., Schouten,
540 S., Werne, J.P.: The vertical distribution of Thaumarchaeota in the water column
541 of Lake Malawi inferred from core and intact polar tetraether lipids. *Org.*
542 *Geochem.* 132, 37-49, DOI: 10.1016/j.orggeochem.2019.03.004, 2019.
- 543 Nakagawa, T., Kitagawa, H., Yasuda, Y., Tarasov, P.E., Nishida, K., Gotanda, K.,
544 Sawai, Y.: Asynchronous Climate Changes in the North Atlantic and Japan
545 During the Last Termination. *Science* 299, 688-691, DOI:
546 10.1126/science.1078235, 2003.
- 547 Nakagawa, T., Tarasov, P.E., Kitagawa, H., Yasuda, Y., Gotanda, K.: Seasonally
548 specific responses of the East Asian monsoon to deglacial climate changes.
549 *Geology* 34, 521-524, DOI: 10.1130/G217641, 2006.
- 550 Ning, D., Zhang, E., Shulmeister, J., Chang, J., Sun, W., Ni, Z.: Holocene mean
551 annual air temperature (MAAT) reconstruction based on branched glycerol
552 dialkyl glycerol tetraethers from Lake Ximenglongtan, southwestern China. *Org.*
553 *Geochem.* 133, 65-76, DOI: 10.1016/j.orggeochem.2019.05.003, 2019.
- 554 Pearson, E.J., Juggins, S., Talbot, H.M., Weckstrom, J., Rosen, P., Ryves, D.B.,
555 Roberts, S.J., Schmidt, R.: A lacustrine GDGT-temperature calibration from the
556 Scandinavian Arctic to Antarctic: Renewed potential for the application of
557 GDGT-paleothermometry in lakes. *Geochim. Cosmochim. Ac.* 75, 6225-6238,
558 DOI: 10.1016/j.gca.2011.07.042, 2011.
- 559 Pitcher, A., Hopmans, E.C., Mosier, A.C., Park, S.-J., Rhee, S.-K., Francis, C.A.,
560 Schouten, S., Sinninghe Damsté J.S.: Core and Intact Polar Glycerol
561 Dibiphytanyl Glycerol Tetraether Lipids of Ammonia-Oxidizing Archaea
562 Enriched from Marine and Estuarine Sediments. *Appl. Environ. Microb.* 77,
563 3468, DOI: 10.1128/AEM.02758-10, 2011.
- 564 Powers, L., Werne, J.P., Vanderwoude, A.J., Sinninghe Damsté J.S., Hopmans, E.C.,
565 Schouten, S.: Applicability and calibration of the TEX₈₆ paleothermometer in
566 lakes. *Org. Geochem.* 41, 404-413, DOI: 10.1016/j.orggeochem.2009.11.009,
567 2010.



- 568 Powers, L.A., Werne, J.P., Johnson, T.C., Hopmans, E.C., Damsté, J.S.S., Schouten, S.:
569 Crenarchaeotal membrane lipids in lake sediments: A new paleotemperature
570 proxy for continental paleoclimate reconstruction? *Geology* 32, 613-616, DOI:
571 10.1130/G20434.1, 2004.
- 572 R Development Core Team, 2013. R: A language and environment for statistical
573 computing, R Foundation for Statistical Computing, Vienna, Austria.
- 574 Rashid, H., Flower, B.P., Poore, R.Z., Quinn, T.M.: A ~25 ka Indian Ocean monsoon
575 variability record from the Andaman Sea. *Quaternary. Sci. Rev.* 26, 2586-2597,
576 DOI: 10.1016/j.quascirev.2007.07.002, 2007.
- 577 Reimer, P.J., Bard, E., Bayliss, A., Beck, J.W., Blackwell, P.G., Ramsey, C.B., Buck,
578 C.E., Cheng, H., Edwards, R.L., Friedrich, M.: IntCal13 and Marine13
579 radiocarbon age calibration curves 0–50,000 years cal BP. *Radiocarbon* 55,
580 1869-1887, DOI: 10.2458/azu_js_rc.55.16947, 2013.
- 581 Russell, J.M., Hopmans, E.C., Loomis, S.E., Liang, J., Sinninghe Damsté J.S.:
582 Distributions of 5- and 6-methyl branched glycerol dialkyl glycerol tetraethers
583 (brGDGTs) in East African lake sediment: Effects of temperature, pH, and new
584 lacustrine paleotemperature calibrations. *Org. Geochem.* 117, 56-69, DOI:
585 10.1016/j.orggeochem.2017.12.003, 2018.
- 586 Saraswat, R., Lea, D.W., Nigam, R., Mackensen, A., Naik, D.K.: Deglaciation in the
587 tropical Indian Ocean driven by interplay between the regional monsoon and
588 global teleconnections. *Earth. Planet. Sc. Lett.* 375, 166-175, DOI:
589 10.1016/j.epsl.2013.05.022, 2013.
- 590 Schouten, S., Hopmans, E.C., Schefuß E., Sinninghe Damsté J.S.: Distributional
591 variations in marine crenarchaeotal membrane lipids: a new tool for
592 reconstructing ancient sea water temperatures? *Earth. Planet. Sc. Lett.* 204,
593 265-274, DOI: 10.1016/S0012-821X(02)00979-2, 2002.
- 594 Schouten, S., Hopmans, E.C., Sinninghe Damsté J.S.: The organic geochemistry of
595 glycerol dialkyl glycerol tetraether lipids: A review. *Org. Geochem.* 54, 19-61,
596 DOI: 10.1016/j.orggeochem.2012.09.006, 2013.
- 597 Schouten, S., Rijpstra, W.I.C., Durisch-Kaiser, E., Schubert, C.J., Sinninghe Damsté



- 598 J.S.: Distribution of glycerol dialkyl glycerol tetraether lipids in the water
599 column of Lake Tanganyika. *Org. Geochem.* 53, 34-37, DOI:
600 10.1016/j.orggeochem.2012.01.009, 2012.
- 601 Sinha, A., Kathayat, G., Cheng, H., Breitenbach, S.F.M., Berkelhammer, M.,
602 Mudelsee, M., Biswas, J., Edwards, R.L.: Trends and oscillations in the Indian
603 summer monsoon rainfall over the last two millennia. *Nat. Commun.* 6, DOI:
604 10.1038/ncomms7309, 2015.
- 605 Sinha, A., Stott, L., Berkelhammer, M., Cheng, H., Edwards, R.L., Buckley, B.,
606 Aldenderfer, M., Mudelsee, M.: A global context for megadroughts in monsoon
607 Asia during the past millennium. *Quaternary. Sci. Rev.* 30, 47-62, DOI:
608 10.1016/j.quascirev.2010.10.005, 2011.
- 609 Sinninghe Damsté J.S., Ossebaar, J., Abbas, B., Schouten, S., Verschuren, D.: Fluxes
610 and distribution of tetraether lipids in an equatorial African lake: Constraints on
611 the application of the TEX₈₆ palaeothermometer and BIT index in lacustrine
612 settings. *Geochim. Cosmochim. Ac.* 73, 4232-4249, DOI:
613 10.1016/j.gca.2009.04.022, 2009.
- 614 Sinninghe Damsté J.S., Ossebaar, J., Schouten, S., Verschuren, D.: Distribution of
615 tetraether lipids in the 25-ka sedimentary record of Lake Challa: extracting
616 reliable TEX₈₆ and MBT/CBT palaeotemperatures from an equatorial African
617 lake. *Quaternary. Sci. Rev.* 50, 43-54, DOI: 10.1016/j.quascirev.2012.07.001,
618 2012a.
- 619 Sinninghe Damsté J.S., Rijpstra, W.I.C., Hopmans, E.C., Jung, M.-Y., Kim, J.-G.,
620 Rhee, S.-K., Stieglmeier, M., Schleper, C.: Intact Polar and Core Glycerol
621 Dibiphytanyl Glycerol Tetraether Lipids of Group I.1a and I.1b *Thaumarchaeota*
622 in Soil. *Appl. Environ Microb* 78, 6866-6874, DOI: 10.1128/AEM.01681-12,
623 2012b.
- 624 Stebich, M., Rehfeld, K., Schlütz, F., Tarasov, P.E., Liu, J., Mingram, J.: Holocene
625 vegetation and climate dynamics of NE China based on the pollen record from
626 Sihailongwan Maar Lake. *Quaternary. Sci. Rev.* 124, 275-289, DOI:
627 10.1016/j.quascirev.2015.07.021, 2015.



- 628 Sun, Q., Chu, G., Xie, M., Ling, Y., Su, Y., Zhu, Q., Shan, Y., Liu, J.: Long-chain
629 alkenone-inferred temperatures from the last deglaciation to the early Holocene
630 recorded by annually laminated sediments of the maar lake Sihailongwan,
631 northeastern China. *Holocene* 28, 1173-1180, DOI: 10.1177/0959683618761546,
632 2018.
- 633 Sun, W., Zhang, E., Shulmeister, J., Bird, M.I., Chang, J., Shen, J.: Abrupt changes in
634 Indian summer monsoon strength during the last deglaciation and early Holocene
635 based on stable isotope evidence from Lake Chenghai, southwest China.
636 *Quaternary. Sci. Rev.* 218, 1-9, DOI: 10.1016/j.quascirev.2019.06.006, 2019.
- 637 Tian, L., Wang, M., Zhang, X., Yang, X., Zong, Y., Jia, G., Zheng, Z., Man, M.:
638 Synchronous change of temperature and moisture over the past 50 ka in
639 subtropical southwest China as indicated by biomarker records in a crater lake.
640 *Quaternary. Sci. Rev.* 212, 121-134, DOI: 10.1016/j.quascirev.2019.04.003,
641 2019.
- 642 Tierney, J.E., Russell, J.M., Huang, Y., Damsté J.S.S., Hopmans, E.C., Cohen, A.S.:
643 Northern Hemisphere controls on tropical southeast African climate during the
644 past 60,000 years. *Science* 322, 252-255, DOI: 10.1126/science.1160485, 2008.
- 645 Tierney, J.E., Russell, J.M., Eggermont, H., Hopmans, E.C., Verschuren, D., Damste,
646 J.S.S.: Environmental controls on branched tetraether lipid distributions in
647 tropical East African lake sediments. *Geochim. Cosmochim. Ac.* 74, 4902-4918,
648 DOI: 10.1016/j.gca.2010.06.002, 2010.
- 649 Wan, G.J., Chen, J.A., Wu, F.C., Xu, S.Q., Bai, Z.G., Wan, E.Y., Wang, C.S., Huang,
650 R.G., Yeager, K.M., Santschi, P.H.: Coupling between $^{210}\text{Pb}_{\text{ex}}$ and organic matter
651 in sediments of a nutrient-enriched lake: An example from Lake Chenghai, China.
652 *Chem Geol* 224, 223-236, DOI: 10.1016/j.chemgeo.2005.07.025, 2005.
- 653 Wang, H., Dong, H., Zhang, C.L., Jiang, H., Liu, Z., Zhao, M., Liu, W.: Deglacial and
654 Holocene archaeal lipid-inferred paleohydrology and paleotemperature history of
655 Lake Qinghai, northeastern Qinghai-Tibetan Plateau. *Quaternary. Res.* 83,
656 116-126, DOI: 10.1016/j.yqres.2014.10.003, 2015.
- 657 Wang, H., Dong, H., Zhang, C.L., Jiang, H., Zhao, M., Liu, Z., Lai, Z., Liu, W.: Water



- 658 depth affecting thaumarchaeol production in Lake Qinghai, northeastern
659 Qinghai–Tibetan plateau: Implications for paleo lake levels and paleoclimate.
660 Chem. Geol. 368, 76-84, DOI: 10.1016/j.chemgeo.2014.01.009, 2014a.
- 661 Wang, H., He, Y., Liu, W., Zhou, A., Kolpakova, M., Krivonogov, S., Liu, Z.: Lake
662 Water Depth Controlling Archaeal Tetraether Distributions in Midlatitude Asia:
663 Implications for Paleo Lake-Level Reconstruction. Geophys. Res. Lett. 46,
664 5274-5283, DOI: 10.1029/2019GL082157, 2019.
- 665 Wang, H., Leng, Q., Liu, W., Yang, H.: A rapid lake-shallowing event terminated
666 preservation of the Miocene Clarkia Fossil Konservat-Lagerstätte (Idaho, USA).
667 Geology 45, 239-242, DOI: 10.1130/G38434.1, 2017a.
- 668 Wang, M., Zheng, Z., Man, M., Hu, J., Gao, Q.: Branched GDGT-based
669 paleotemperature reconstruction of the last 30,000 years in humid monsoon
670 region of Southeast China. Chem. Geol. 463, 94-102, DOI:
671 10.1016/j.chemgeo.2017.05.014, 2017b.
- 672 Wang, Q., Yang, X., Anderson, N.J., Zhang, E., Li, Y.: Diatom response to climate
673 forcing of a deep, alpine lake (Lugu Hu, Yunnan, SW China) during the Last
674 Glacial Maximum and its implications for understanding regional monsoon
675 variability. Quaternary. Sci. Rev. 86, 1-12, DOI: 10.1016/j.quascirev.2013.12.024,
676 2014b.
- 677 Wang, S., Dou, H., 1998. Lakes in China. Science Press, Beijing, China (in Chinese).
- 678 Weijers, J.W.H., Schouten, S., Spaargaren, O.C., Damste, J.S.S.: Occurrence and
679 distribution of tetraether membrane lipids in soils: Implications for the use of the
680 TEX₈₆ proxy and the BIT index. Org. Geochem. 37, 1680-1693, DOI:
681 10.1016/j.orggeochem.2006.07.018, 2006.
- 682 Wu, D., Chen, X., Lv, F., Brenner, M., Curtis, J., Zhou, A., Chen, J., Abbott, M., Yu, J.,
683 Chen, F.: Decoupled early Holocene summer temperature and monsoon
684 precipitation in southwest China. Quaternary. Sci. Rev. 193, 54-67, DOI:
685 10.1016/j.quascirev.2018.05.038, 2018.
- 686 Wu, D., Zhou, A., Chen, X., Yu, J., Zhang, J., Sun, H.: Hydrological and ecosystem
687 response to abrupt changes in the Indian monsoon during the last glacial, as



688 recorded by sediments from Xingyun Lake, Yunnan, China. *Palaeogeogr.*
689 *Palaeocl.* 421, 15-23, DOI: 10.1016/j.palaeo.2015.01.005, 2015.

690 Wu, J., Gagan, M.K., Jiang, X., Xia, W., Wang, S.: Sedimentary geochemical
691 evidence for recent eutrophication of Lake Chenghai, Yunnan, China. *J.*
692 *Paleolimnol.* 32, 85-94, 2004.

693 Yao, Y., Zhao, J., Bauersachs, T., Huang, Y.: Effect of water depth on the TEX₈₆ proxy
694 in volcanic lakes of northeastern China. *Org. Geochem.* 129, 88-98, DOI:
695 10.1016/j.orggeochem.2019.01.014, 2019.

696 Zhang, E., Chang, J., Cao, Y., Sun, W., Shulmeister, J., Tang, H., Langdon, P.G., Yang,
697 X., Shen, J.: Holocene high-resolution quantitative summer temperature
698 reconstruction based on subfossil chironomids from the southeast margin of the
699 Qinghai-Tibetan Plateau. *Quaternary. Sci. Rev.* 165, 1-12, DOI:
700 10.1016/j.quascirev.2017.04.008, 2017a.

701 Zhang, E., Chang, J., Shulmeister, J., Langdon, P., Sun, W., Cao, Y., Yang, X., Shen, J.:
702 Summer temperature fluctuations in Southwestern China during the end of the
703 LGM and the last deglaciation. *Earth. Planet. Sc. Lett.* 509, 78-87, DOI:
704 10.1016/j.epsl.2018.12.024, 2019.

705 Zhang, E., Sun, W., Chang, J., Ning, D., Shulmeister, J.: Variations of the Indian
706 summer monsoon over the last 30 000 years inferred from a pyrogenic carbon
707 record from south-west China. *J. Quaternary. Sci.* 33, 131-138, DOI:
708 10.1002/jqs.3008, 2018.

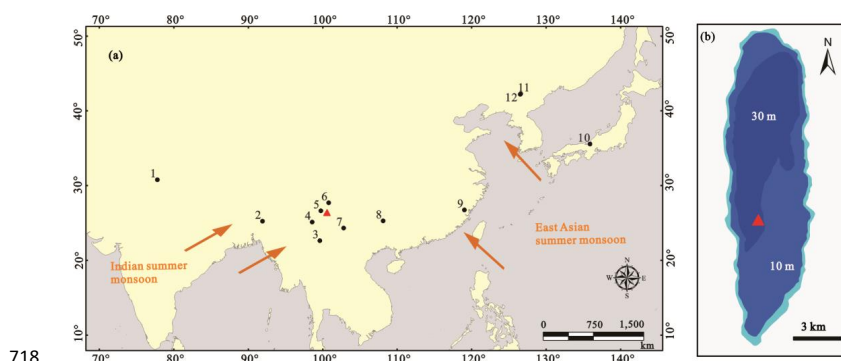
709 Zhang, E., Zhao, C., Xue, B., Liu, Z., Yu, Z., Chen, R., Shen, J.: Millennial-scale
710 hydroclimate variations in southwest China linked to tropical Indian Ocean since
711 the Last Glacial Maximum. *Geology* 45, 435-438, DOI: 10.1130/G38309.1,
712 2017b.

713 Zheng, Y., Pancost, R.D., Naafs, B.D.A., Li, Q., Liu, Z., Yang, H.: Transition from a
714 warm and dry to a cold and wet climate in NE China across the Holocene. *Earth.*
715 *Planet. Sc. Lett.* 493, 36-46, DOI: 10.1016/j.epsl.2018.04.019, 2018.

716

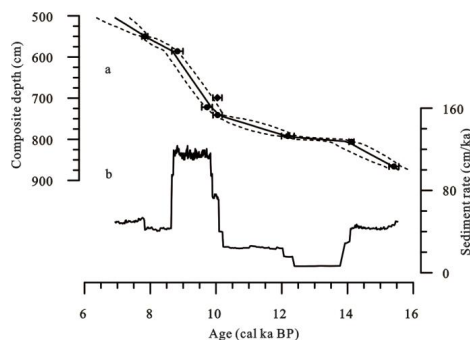


717 **Figure captions**



718

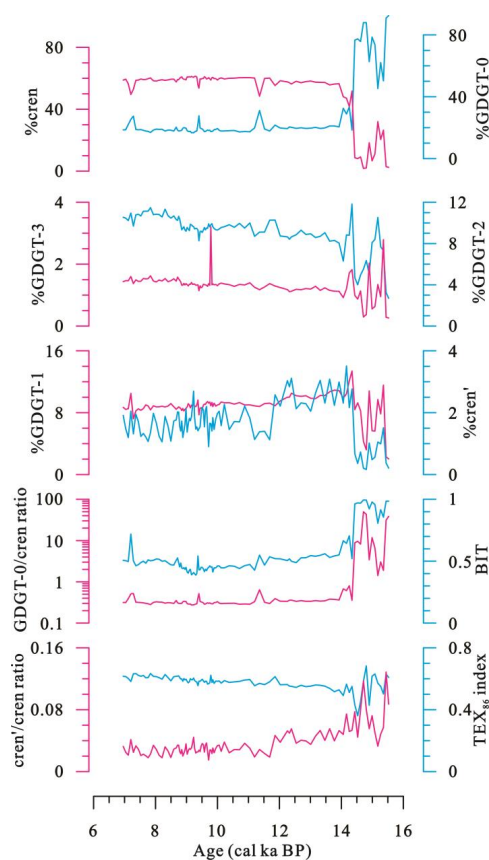
719 **Fig. 1.** (a) Map showing the location of Lake Chenghai in southwest China (triangle)
720 and other sites (circles) mentioned in the text: 1. Bittoo Cave (Kathayat et al., 2016);
721 Mawmluh Cave (Dutt et al., 2015); 3. Lake Ximenglongtan (Ning et al., 2019); 4.
722 Lake Tengchongqinghai (Zhang et al., 2017b; Li et al., 2018; Tian et al., 2019); 5.
723 Lake Tiancai (Zhang et al., 2017a, 2019); 6. Lake Lugu (Wang et al., 2014); 7. Lake
724 Xingyun (Wu et al., 2015, 2018); 8. Dongge Cave (Dykoski et al., 2005); 9. Peat bog
725 Shuizhuyang (Wang et al., 2017b); 10. Lake Suigetsu (Nakagawa et al., 2003, 2006);
726 11. Lake Sihailongwan (Stebich et al., 2015; Sun et al., 2018), 12. Gushantun peat bog
727 (Zheng et al., 2018). Arrows indicate the dominant atmospheric circulation systems in
728 the region. (b) The triangle in panel b indicates the location of core CH2016 in Lake
729 Chenghai.



730

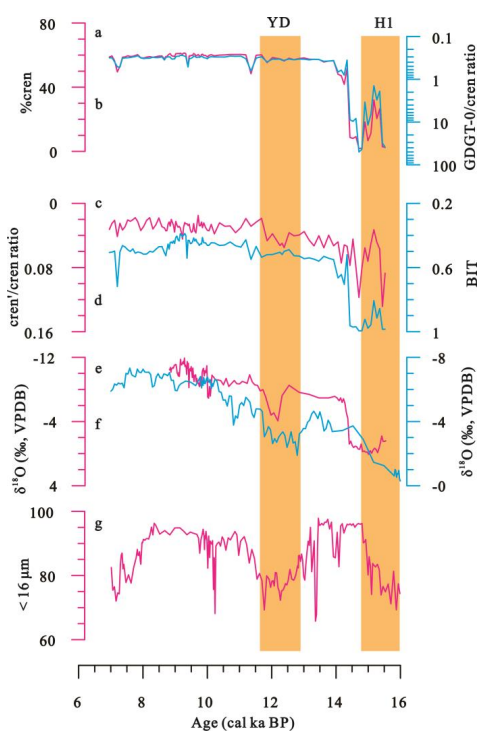


731 **Fig. 2.** (a) Age-depth model for the Lake Chenghai sediment core produced by Bacon
732 software (Blaauw and Andres Christen, 2011; Sun et al., 2019). Dotted lines indicate
733 the 95% confidence range and the solid line indicates the weighted mean ages for
734 each depth, error bars indicate the standard deviation range (2σ) of the calibrated
735 radiocarbon dates. (b) estimated sedimentation rate (Sun et al., 2019).



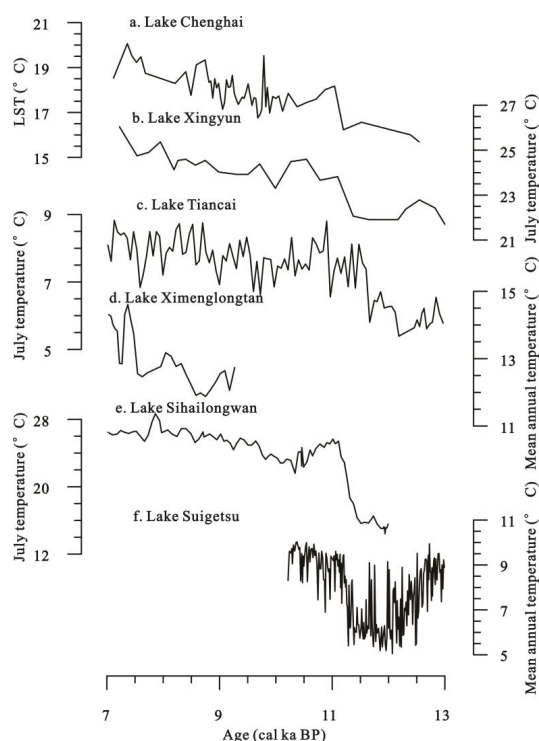
736

737 **Fig. 3.** Variations in the relative isoGDGT distribution and isoGDGTs-based proxies
738 of the Lake Chenghai sediments.



739

740 **Fig. 4.** Comparison of the isoGDGT-based lake-level record from Lake Chenghai (a-d)
741 with the $\delta^{18}\text{O}$ record of carbonate finer in grain size than $63\ \mu\text{m}$ from Lake Chenghai
742 (e, Sun et al., 2019), the stalagmite $\delta^{18}\text{O}$ records from Mawmluh Cave in northeast
743 Indian (f, Dutt et al., 2015); and grain-size record from Lake Tengchongqinghai (g,
744 Zhang et al., 2017). The shading is utilised to represent ‘cold’ events in the North
745 Atlantic.



746

747 **Fig. 5.** A comparison of TEX₈₆-based lake surface temperature of Lake Chenghai (a)
748 with other paleotemperature records. July temperature reconstructed from pollen
749 record from Lake Xingyun (b, Wu et al., 2018) and subfossil chironomids from Lake
750 Tiancai (c, Zhang et al., 2017a, 2019); mean annual temperature reconstructed from
751 Lake Ximenglongtan based on brGDGTs (d, Ning et al., 2019); July temperature
752 reconstructed from pollen record from Lake Sihailongwan (e, Stebich et al., 2015);
753 and pollen reconstructed mean annual temperature from Lake Suigetsu (f, Nakagawa
754 et al., 2003).

755